Pure Appl. Geophys.

https://doi.org/10.1007/s00024-024-03532-x

Pure and Applied Geophysics

Exploring Electromagnetic Wave Propagation Through the Ionosphere Over Seismic Active Zones

Husan Eshkuvatov,[1,2,3] Bobomurat Ahmedov,[4] Munawar Shah,[5] Dilfuza Begmatova,[1] Punyawi Jamjareegulgarn,[6] and Angela Melgarejo-Morales[7]

Abstract—This study presents an analytical solution for the electric current formation in the lower ionosphere as a result of charged aerosols being ejected from the ground before the earthquakes. The impact of ionosphere-related processes on radio wave propagation through the atmosphere is explored by investigating the resulting energy losses of electromagnetic waves traversing this ionospheric layer. Theoretical considerations suggest that these processes may generate detectable electromagnetic signals, offering insights into seismic precursors. The effects of electron density inhomogeneities in the upper ionospheric layers on electromagnetic wave properties such as group delay, Faraday rotation, and Doppler frequency shift are examined. Understanding these effects aims to improve ionospheric monitoring techniques to detect pre-earthquake disturbances. To validate the theoretical findings, a comparison is made with the empirical data from various sources, including VLF transmitters and GPS-TEC measurements. This comparative analysis underscores the potential of electromagnetic phenomena as credible indicators of impending seismic events.

Keywords: Earthquake precursors, Atmosphere, Ionosphere, Electromagnetic waves, Faraday rotation.

1. Introduction

The study of ionospheric precursors has garnered considerable attention for earthquake prediction. Recently, the issue of how earthquakes might affect the ionosphere's characteristics was debated by numerous authors. Although some theories have been put forth that involve direct coupling from the Earth's surface to the lower ionosphere through electric currents (Pulinets & Boyarchuk, 2004; Sorokin & Yaschenko, 2000) or the triggering of atmospheric gravity waves by gas releases or thermal anomalies. However, the precise mechanism linking ground-level electromagnetic signals with ionospheric anomalies remains elusive (Molchanov & Hayakawa, 2001; Shvets et al., 2004).

The theoretical structure for anticipating precursor signals remains unknown due to the complexity of the underlying physical processes. This complexity makes it challenging to differentiate precursor signals from those generated by other activities. Currently, empirical studies of ionospheric precursor signals provide our primary means of investigation. Of particular significance is the release of soil aerosols into the atmosphere concurrent with seismic activity, which plays a special role in ionospheric disturbances preceding earthquakes. The transit of charged aerosols vertically alters the global atmosphere–ionosphere electric circuit, resulting in external currents in the lower atmosphere.

Sorokin et al. (2001) provided a model of the coupling between the lower and upper ionospheres, offering insights into the causal relation underlying seismo-ionospheric interactions. Similarly, Rapoport et al. (2006) proposed a 3D model for the production

[1] National University of Uzbekistan, University St. 4, 100174 Tashkent, Uzbekistan. E-mail: husan@astrin.uz; drdf123@gmail.com

[2] Ulugh Beg Astronomical Institute, Astronomy Str. 33, 100052 Tashkent, Uzbekistan.

[3] Tashkent Institute of Irrigation and Agricultural Mechanization Engineers, Kori Niyoziy 39, 100000 Tashkent, Uzbekistan.

[4] Institute of Fundamental and Applied Research, National Research University TIIAME, Kori Niyoziy 39, 100000 Tashkent, Uzbekistan. E-mail: ahmedov@astrin.uz

[5] School of Surveying and GeoInformatics, Tongji University, Shanghai, China. E-mail: shahmunawar1@gmail.com

[6] King Mongkut's Institute of Technology Ladkrabang, Prince of Chumphon Campus, Chumphon 86160, Thailand. E-mail: kjpunyaw@gmail.com

[7] SCiESMEX, LANCE, Instituto de Geofísica, Unidad Michoacán, Universidad Nacional Autónoma de México, C.P. 58190 Morelia, Michoacán, México. E-mail: angela@igeofisica.unam.mx

of an electrostatic field in the lithosphere, atmosphere, and ionosphere system in the presence of external currents. Several studies have investigated the production of DC electric fields over seismic zones in the mid-latitude ionosphere (Sorokin, 2007; Sorokin & Yaschenko, 2000; Sorokin et al., 2005a, 2005b, 2006a, 2006b). Additionally, Sorokin (2007) and Sorokin et al. (1998) have described the development of small-scale, geomagnetic field-aligned plasma density inhomogeneities in the upper ionosphere, providing a physical model for their generation.

In recent years, seismic disturbances in VLF radio signals have been observed (Biagi et al., 2005, 2007; Hayakawa, 2007; Hayakawa et al., 2006, 2007; Horie et al., 2007a, 2007b; Kasahara et al., 2008; Molchanov & Hayakawa, 2008; Rozhnoi et al., 2007). These disturbances seem to arise from variations in the lower atmosphere/ionosphere of the area where the propagation of the radio signals happens. According to recent models, these variations stem from turbulent atmospheric gravity waves of low amplitude generated near the ground surface by pre-seismic and postseismic processes, such as gas and water releases in seismic active regions (Mareev et al., 2002; Molchanov et al., 2006).

For instance, in Tashkent Uzbekistan, an earthquake struck on August 22, 2008. The Ulugh Beg Astronomical Institute's VLF receiver, located a few kilometers from the epicenter, detected anomalies in the TEC concentration before, during, and after the earthquake (Tojiev et al., 2013). In the region of the earthquake's epicenter, the routes of the VLF radio signals picked up by the Tashkent Pass VLF receiver were compiled. The findings of the investigation into potential seismic impacts on the VLF radio signals captured at the Tashkent station are also provided here (Tojiev et al., 2014).

The paper is organized as follows. The first section focuses on the study of how seismic processes influence electromagnetic wave propagation through the ionosphere by modifying its properties. Phenomena such as plasma density inhomogeneities in the upper ionosphere can induce modulations of wave parameters, which may be seen during radiolocation, satellite observations, etc. Section 2 delves into the influence of DC electric field generated in the mid-latitude ionosphere by external electric currents originating from earthquakes on electromagnetic waves. This section explores electromagnetic wave propagation through the horizontal distribution of the ionosphere scalar potential caused by seismic activity. In Sect. 3, plasma density inhomogeneities aligned along the geomagnetic field are examined. Three measurable effects on electromagnetic wave propagation resulting from inhomogeneities approximated as periodic functions are discussed: the group delay of the wave in Sect. 3.1, Faraday rotation in Sect. 4.1, and Doppler shift in Sect. 4.2. Subsequently, the application of the obtained results to GPS monitoring of ionospheric disturbances produced in the earthquake preparation period is considered. In Sect. 5, VLF radio signal anomalies associated with the Tashkent earthquake that occurred on 22 August, 2008 are discussed. In the final section, the paper highlights and discusses the key findings obtained throughout the study.

2. *Energy Losses Due to Lower Ionosphere Currents*

The equations in Sorokin et al. (2006b) for the horizontal scalar potential distribution in the mid-latitude ionosphere layer are investigated. Potential distribution is assumed to be connected with the presence of external currents near the ground.

These currents consist of charged aerosol injections and vertical convective motions of gases in the lower atmosphere, on electromagnetic wave energy losses. These currents are integral components of the Earth's atmosphere–ionosphere electric circuit, as depicted in Fig. 1, a commonly referenced graphical model in the literature. In Sorokin et al. (2006b), numerical solutions were derived for scalar potential under the assumption of a large-scale axial symmetric external current. However, the focus lies in an analytical solution for the scalar potential through a specialized formulation of the the electric current expression.

Using the continuity equation $\nabla(\mathbf{J} + \mathbf{J}_e) = 0$ and Ohm's law for ionosphere electric current $\mathbf{J} = \sigma\mathbf{E} = -\sigma\nabla\boldsymbol{\phi}$, one can obtain the following equation for the atmosphere scalar potential ϕ

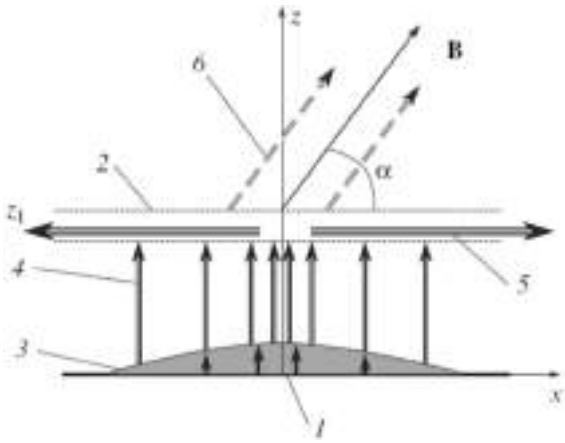

Figure 1
Scheme of the model used for the calculations of current and field in the atmosphere–ionosphere electric circuit: 1. Earth's surface; 2. Conducting ionosphere; 3. Zone of upward convection of charged aerosols and external electric currents formation; 4. Conductivity current in the atmosphere; 5. Conductivity current flowing along the ionosphere; 6. Field-aligned electric current

$$\frac{d}{dz}\left[\sigma(z)\frac{d\phi}{dz} - j_e(x,y,z)\right] = 0, \tag{1}$$

which after choosing corresponding boundary conditions for the atmosphere

$$\phi|_{z=0} = 0,$$

$$\sigma_1 \frac{d\phi}{dz}|_{z=z_1-0} = 2\Sigma_P\left(\frac{1}{\sin^2\alpha}\frac{\partial^2\phi_1}{\partial x^2} + \frac{\partial^2\phi_1}{\partial y^2}\right) - \frac{\phi_1}{\rho} \tag{2}$$

looks like

$$\frac{1}{\sin^2\alpha}\frac{\partial^2\phi_1(x,y)}{\partial x^2} + \frac{\partial^2\phi_1(x,y)}{\partial y^2} = -\frac{1}{2\Sigma_P\rho}\int_0^{z_1}\frac{j_e(x,y,z)}{\sigma(z)}dz, \tag{3}$$

$$\rho = \int_0^{z_1}\frac{dz}{\sigma(z)}.$$

It is assumed that the thin conductive ionosphere layer is located at a height z_1, above Earth's surface. Here $j_e(x,y,z)$ is the extraneous electric current, $\sigma(z)$ is the altitude dependent atmospheric conductivity, Σ_P is the integral Pedersen conductivity of the ionosphere. In chosen Cartesian coordinates (x,y,z), the z-axis is directed vertically upward, with the origin located on the Earth's conductive surface. Ahomogeneous magnetic field **B** is assumed to be directed at the angle α with respect to the x-axis.

For simplicity of analytical calculations, we will assume external electric current $j_e(x,y,z)$ to be as

$$j_e(x,y,z) = j_{e0}\exp\left(-\frac{z}{h_j}\right)\exp\left(-\frac{x}{l}\right)\exp\left(-\frac{y}{l}\right) \tag{4}$$

and

$$\sigma(z) = \sigma_0\exp\left(\frac{z}{h}\right), \tag{5}$$

where l is the characteristic horizontal scale of the process, h_j and h are vertical scalers of external current and atmosphere conductivity changes, respectively. In assumption of the Eqs. (4) and (5), the Eq. (3) for scalar potential will look like

$$\frac{1}{\sin^2\alpha}\frac{\partial^2\phi_1(x,y)}{\partial x^2} + \frac{\partial^2\phi_1(x,y)}{\partial y^2} = b\exp\left(-\frac{x}{l}\right)\exp\left(-\frac{y}{l}\right) \tag{6}$$

with parameter

$$b = -\frac{j_{e0}}{2\Sigma_P\rho\sigma_0}\int_0^{z_1}\exp\left\{-z\left(\frac{1}{h_j}+\frac{1}{h}\right)\right\}dz$$

$$= \frac{j_{e0}}{2\Sigma_P\rho\sigma_0}\frac{h_j h}{h_j + h}\left[\exp\left\{-z_1\left(\frac{1}{h_j}+\frac{1}{h}\right)\right\} - 1\right]. \tag{7}$$

Exact solution of Eq. (6) can be written as

$$\phi_1 = \frac{bl^2\sin^2\alpha}{1+\sin^2\alpha}\exp\left(-\frac{x}{l}\right)\exp\left(-\frac{y}{l}\right). \tag{8}$$

The dependence of the scalar potential in the solution (8) from the angle α and from the maximum value of the external current is presented in Figs. 2 and 3. The following are typical parameters for ionospheric plasma:$\Sigma_P = 10^{12}$ cm/s,$\sigma_0 = 2\times10^{-4}\mathrm{s}^{-1}$,$h = 5$ km,-,$z_1 = 10$ km,$l = 100$ km. For Fig. 2, $j_{e0} = 4\times10^{-10}$ A/cm^2 and for Fig. 3 $\alpha = 45^\circ$ were used. From Fig. 2, one can see that potential significantly enlarges when angle α goes to $\pi/2$, reaching its maximum value at this point. Additionally, Fig. 3 demonstrates that the potential linearly increases with the amplitude of the external current.

Now, knowing the exact expression for scalar potential ϕ_1 one can find the distribution of electric field through the relation $\mathbf{E} = -\nabla\phi$ and then using

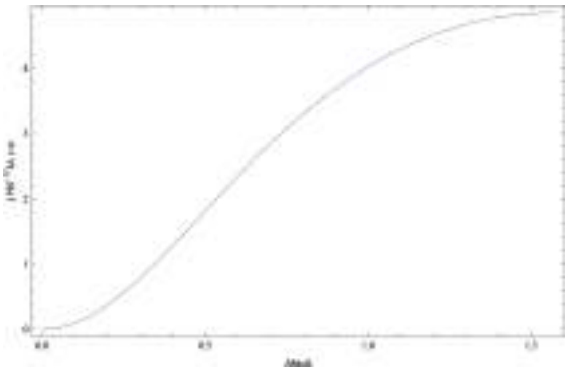

Figure 2
The dependence of the maximum value of scalar potential, arising in the lowest ionosphere, from the angle α between the magnetic field and x axis. (α changes from 0 to 90°)

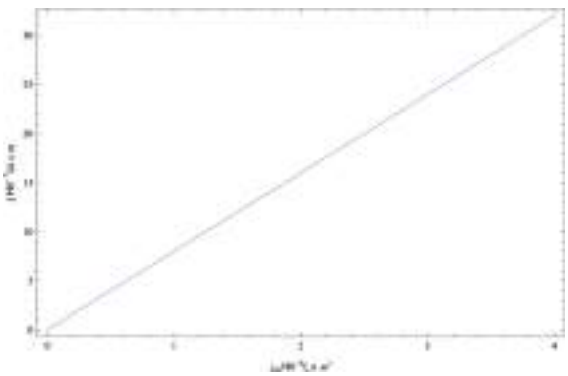

Figure 3
The dependence of the magnitude of the scalar potential, arising in the lowest ionosphere, from the magnitude of external current

Ohm's law the vector of electric current, which will have the following nonvanishing components:

$$j_x = j_y = \frac{\Sigma_P bl \sin^2\alpha}{1+\sin^2\alpha}\exp\left(-\frac{x}{l}\right)\exp\left(-\frac{y}{l}\right). \quad (9)$$

Given that the electric current distribution plays a role in external forces for propagating electromagnetic waves, the presence of such currents will induce power losses of waves. These losses can be determined by:

$$P = \int_V \mathbf{jE} dv, \quad (10)$$

where V represents the volume in which the electric currents are localized, in our case, we choose this volume to have horizontal scales $2l$ and a height of Δz. Assuming that the components of electric vector E_x and E_y in the wave do not depend on coordinates x and y, one can derive the integral for energy losses as:

$$P = \int_{-l}^{l}\int_{-l}^{l}\int_{z_1}^{z_1+\Delta z}(E_x + E_y)\frac{\Sigma_P bl\sin^2\alpha}{1+\sin^2\alpha}\exp\left(-\frac{x}{l}\right)\exp\left(-\frac{y}{l}\right)dxdydz$$
$$= -\frac{\Sigma_P 4bl^3\sin^2\alpha}{1+\sin^2\alpha}sh^2 1(E_x+E_y)\Delta z, \quad (11)$$

And inserting b from Eq. (7), we finally obtain the correlation between the energy losses of electromagnetic waves propagating through the mid-latitude ionosphere and the external current arising before earthquakes as:

$$P = \frac{2j_{e0}l^3\sin^2\alpha sh^2 1}{\rho\sigma_0(1+\sin^2\alpha)}\frac{h_j h}{h_j+h}\left[\exp\left\{-z_1\left(\frac{1}{h_j}+\frac{1}{h}\right)\right\}-1\right](E_x + E_y)\Delta z. \quad (12)$$

The detailed analysis of a very large daily dataset received from GPS may potentially reveal isolated evidence for anomalous signals, particularly in changes in radio signal intensity in the days preceding an earthquake. The quality and spatial density of the GPS dataset obtained from daily monitoring at GPS stations provide an opportunity to effectively test for such situations.

3. *Wave Effects Due to Plasma Density Inhomogeneities*

Seismic activity often triggers the formation of ionospheric plasma density irregularities. In particular, according to COSMOS-1809 satellite data (Chmyrev et al., 1997), electron density inhomogeneities with spatial scales ≤ 10 km arise in the upper ionosphere before an earthquake. Analysis of a number of observational data has revealed that these seismic-related plasma density irregularities typically exhibit characteristic spatial scales of $l \sim 4-10$ km and magnitudes $dN_e/N_e \sim 4-10\%$. As it is assumed by Sorokin et al. (1998), ionospheric plasma density irregularities are produced as the result of the formation of the field-aligned currents with transverse scales ≤ 10 km, which are excited in the lower

ionosphere. These currents, in turn, originate from small-scale conductivity variations. A graphical representation of upper ionospheric inhomogeneities is depicted in Fig. 4 (adapted from the paper by Sorokin et al. (1998)).

Plasma density inhomogeneities in the ionosphere have the potential to significantly impact the parameters of radio waves propagating through it. In this study, we will consider some of these parameters and approximate the effects of field-aligned inhomogeneities associated with acoustic-gravity waves instability as:

$$\Delta N = \Delta N\prime \cdot \sin^2 \frac{2\pi}{l} x, \tag{13}$$

where x axis is chosen to be horizontal, l is the spatial scale of inhomogeneities. The electron density profile of the unperturbed ionosphere is available at http://www.ngdc.noaa.gov/. It is assumed that $\Delta N\prime$ being about 5% from the unperturbed value of electron density depends on the height in the same way.

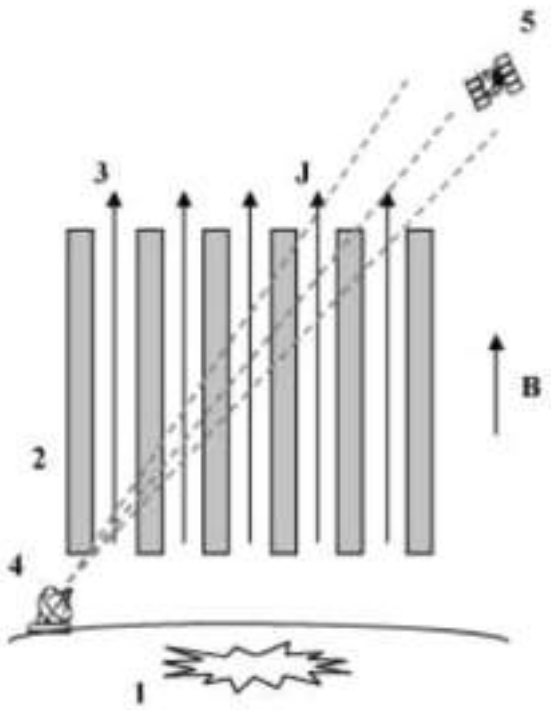

Figure 4
The scheme of GPS monitoring of plasma density inhomogeneities: 1. Earthquake; 2. Plasma density inhomogeneities along geomagnetic field; 3. Field-aligned electric currents; 4. Ground-based GPS receiver; 5. GPS satellite

3.1. Group Delay of the Radio Wave

The first effect which will be considered is the "group delay" of radio waves propagating through the ionosphere. Inhomogeneities in the propagation medium trigger changes in the group velocity of the radio signal, deviating from the speed of light in a vacuum. This deviation becomes significant in radiolocation scenarios, as the apparent distance from the object (referred to as the group path) differs from the real distance. In isotropic plasma, the apparent distance is defined by the equation.

$$L = c \int_0^{s(R)} \frac{ds}{g}, \tag{14}$$

where $g = d\omega/dk$ is the group velocity of the signal which in the isotropic plasma is equal to

$$g = c\sqrt{1 - 4\pi e^2 N/(m\omega^2)}. \tag{15}$$

In cold isotropic plasma electron concentration N is connected with the parameter $v = \varepsilon - 1$ containing the dielectric permittivity ε through the relation

$$v = -\frac{4\pi e^2}{m\omega^2} N(\mathbf{r}). \tag{16}$$

Taking into account Eq. (16) and extending expression (14) in a series in the approximation of small inhomogeneities N, one can find the following expression for the group way as below.

$$L = L_0 + L_1 + \ldots = R - \frac{1}{2}\int_0^R v(s\prime)ds\prime + \ldots. \tag{17}$$

The R is the absolute value of the vector R which connects radio wave emission and detection points.

Now choose the z axis to be directed upward having 0 in the lowest point of inhomogeneities formation and z_h in its highest point. Then choose an axis $x\prime$ having the same zero point as z directed along plane wave propagation and the angle between $x\prime$ and z axis is β. The spatial scale of inhomogeneities in this direction will be equal to $l/\sin\beta$. One can approximate the unperturbed electron density as $N = N_m e^{-x\prime\cos\beta/\mathrm{H}}$ where N_m is the value of the electron density in the lowest point of inhomogeneities formation H is the characteristic vertical scale. To find the first correction to group way in $x\prime$ direction one should integrate corresponding v along this line.

The value of the frequency v given by (16) and expression (13) (when $\Delta N\prime = 0.05N$) can be inserted into the integral (17) as the following.

$$L_1 = -\frac{1}{2}\left(-\frac{4\pi e^2}{m\omega^2}\right)0.05N_m\int_0^{\frac{z_h}{\cos\beta}} e^{-\frac{x\prime\cos\beta}{H}}\sin^2\left(\frac{2\pi\sin\beta}{l}x'\right)dx'. \tag{18}$$

Averaging (18) in space and taking integral, one could get finally the result.

$$L_1 = \frac{\pi e^2}{m\omega^2}\frac{H}{\cos\beta}0.05N_m\left(1 - e^{-\frac{z_h}{H}}\right), \tag{19}$$

which is in good agreement with the assumption that the wave will go through the inhomogeneities approximately half of the wave's path.

The dependence of L_1 from z_h is graphically represented in Fig. 5 for the following set of typical parameters: $N_m \simeq 10^6\ cm^{-3}$, $f = \omega/2\pi = 1.22 \times 10^9$ Hz, $\beta = 45^\circ$ and $H \simeq 100$ km. In fact, the effect of ionospheric perturbation adds a contribution of the order of several percent to the unperturbed case. As is seen from the Fig. 4, the effect grows logarithmically with the height of the satellite motion.

4. *Pre-Ionospheric Phenomena Associated with a Strong Earthquake in Afghanistan from GNSS Data*

Historically, ionosondes were successfully used to register ionospheric parameters, including the ionospheric plasma frequency. A local ionosonde is capable to provide information about electron density at a certain height of the atmosphere. However, in recent years, ground-based GPS receivers have emerged as alternative and in many respects, preferable tools for monitoring the ionosphere. This shift is attributed to the widespread deployment of GPS stations, surpassing the number of ionosondes globally by at least one order of magnitude. GPS receivers are not only easier to operate but also provide highly reliable information.

GPS receivers measure the slant Total Electron Content (sTEC), which is the integral of electron concentration along the ray path from the ground-based station to the satellite. Thus, sTEC measurements are closely related to the group delay of the wave. sTEC measurements can then be converted to vertical Total Electron Content (vTEC).

Measurements of group delay variations of GPS signal associated with earthquakes have been

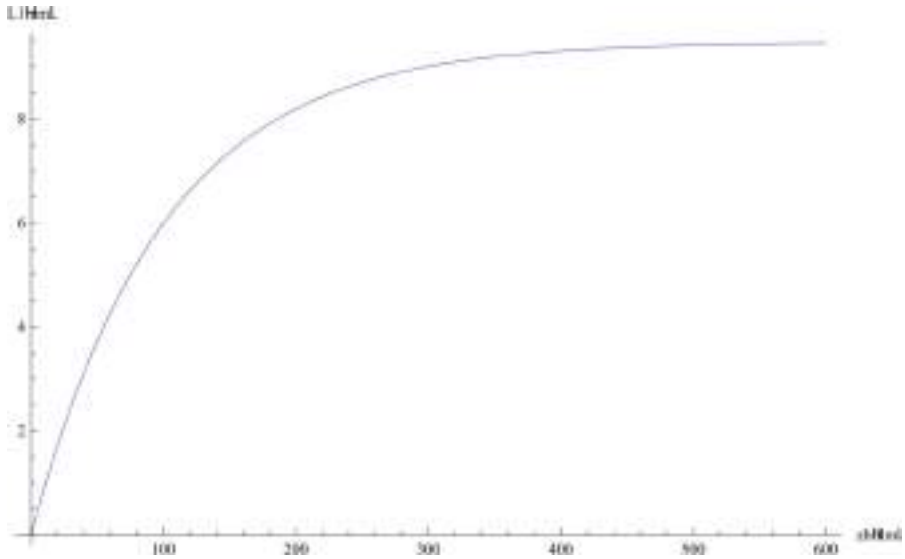

Figure 5
The dependence of the first correction to the group path of the wavepropagating through the inhomogeneities of the highest layer of the ionosphere as a function of height

conducted. For example, in the paper of Calais et al. (1998), group delay changes during the Northridge earthquake of 1994 and a space shuttle launch were analyzed. During the earthquake, observed group delay variations were less than 1 cm, whereas during the shuttle launch, they ranged from $6-10$ cm. The order of L_1 variations obtained in our study is in agreement with these observations. Precise values of L_1 can be obtained using precise characteristics of ionosphere and disturbances. The accuracy of group delay measurements at GPS frequency is typically 5 and10 mm, making variations on the order of several centimeters easily detectable. In the paper of Liu et al. (2004), data from a GPS ground-based receiver were analyzed, and anomalies in Total Electron Content (TEC) before 20 strong earthquakes ($M \geq 6.0$) were identified. It was observed that within 1–7 days before these earthquakes, both lower and upper quasiperiodic anomalies in the Total Electron Concentration were detected.

In our previous papers (Eshkuvatov et al., 2023; Tojiev et al., 2012, 2013, 2014), we identified anomalous TEC signals and observed a significant temporal correlation between these TEC anomalies and the occurrence of earthquakes in Tashkent on 22 August, 2008. The amplitude of the maximum TEC value over Tashkent reached a deviation of $\sim$ 20 30% compared to the nondisturbed initial monthly mean background value one day before and after the earthquake. Notably, at the precise time of the earthquake occurrence, TEC drastically dropped by returning to near-typical value after $\sim$ 5 h. One could attempt to correlate anomalies detected by GPS ground-based stations (described in the paper of Liu et al. (2004)) with those detected by satellite (Sorokin, 2007; Sorokin et al., 1998). In Sorokin et al. (1998), satellites cross the ionosphere at heights on the order of 800 km, while GPS stations measures vTEC, which integrates electron density from the Earth to the GPS satellite at heights around $20,000$ km. It seems to be quite possible that anomalies in electron content detected by ground-based stations result from periodic plasma density inhomogeneities slowly drifting in the upper ionosphere.

A rough analysis can be performed to assess this point of view. The characteristic scale of plasma inhomogeneities measured by crossing satellite is $l \sim 4-10$ km, while the duration of anomalies recorded by the GPS system is typically several hours (Ahmedov et al., 2015; Tojiev et al., 2013). For calculations, a duration of 5 h can be considered. This implies that for correlation between observations, the inhomogeneities should drift through the ionosphere with a velocity $v_{df} \sim 10$ k$m/5$h $= 54$ cm/s. The obtained velocity is of the same order of magnitude as the vertical mass transfer velocity, which is ~ 10 cm/s. The magnitude of the effect measured by crossing satellites is on the order of 10 %. In the graphs presented in Liu et al. (2004) for variations of vTEC observed in September 1999, deviations from the upper and lower boundaries of normal vTEC have the same order of magnitude. The time of crossing satellite observations is about several hours before the earthquake. GPS observations reveal anomalies within several days before earthquakes, but Liu et al. (2004) considered rather strong earthquakes ($M \geq 6.0$) for such variations. A rough analysis suggest the possibility of a correlation between the phenomena described in these two cases. Even if an exact correlation can not be established, it is reasonable to assume that GPS observed anomalies share the same origin as those detected by crossing satellites (Sorokin, 2007; Sorokin et al., 1998).

The new results obtained from the GNSS device installed in Maidanak and Maidantal GPS stations for the Afghanistan M = 6.0 EQ of June 21, 2022 are presented in Fig. 6 and strongly support our previous findings. Similarly, statistical observations indicate that the strong local earthquakes are preceded by ionospheric precursors. The TEC time series were calculated at both sites, revealing anomalous TEC deflection and mostly positive/ negative differential Total Electron Content (dTEC) anomalies using a few days of continuous data associated with the occurrence of earthquakes. However, it is important to note that these anomalies can not be conclusively considered ionospheric precursors of the earthquake due to the high geomagnetic index observed during that period (Shah & Jin, 2015; Shah et al., 2018, 2019a, 2020, 2020a, 2022; Shah et al., 2019b, 2020b, 2021a, 2021b, 2021c, 2023a). The P indicates that the ionospheric precursors were identified 4 days before the Afghanistan earthquake.

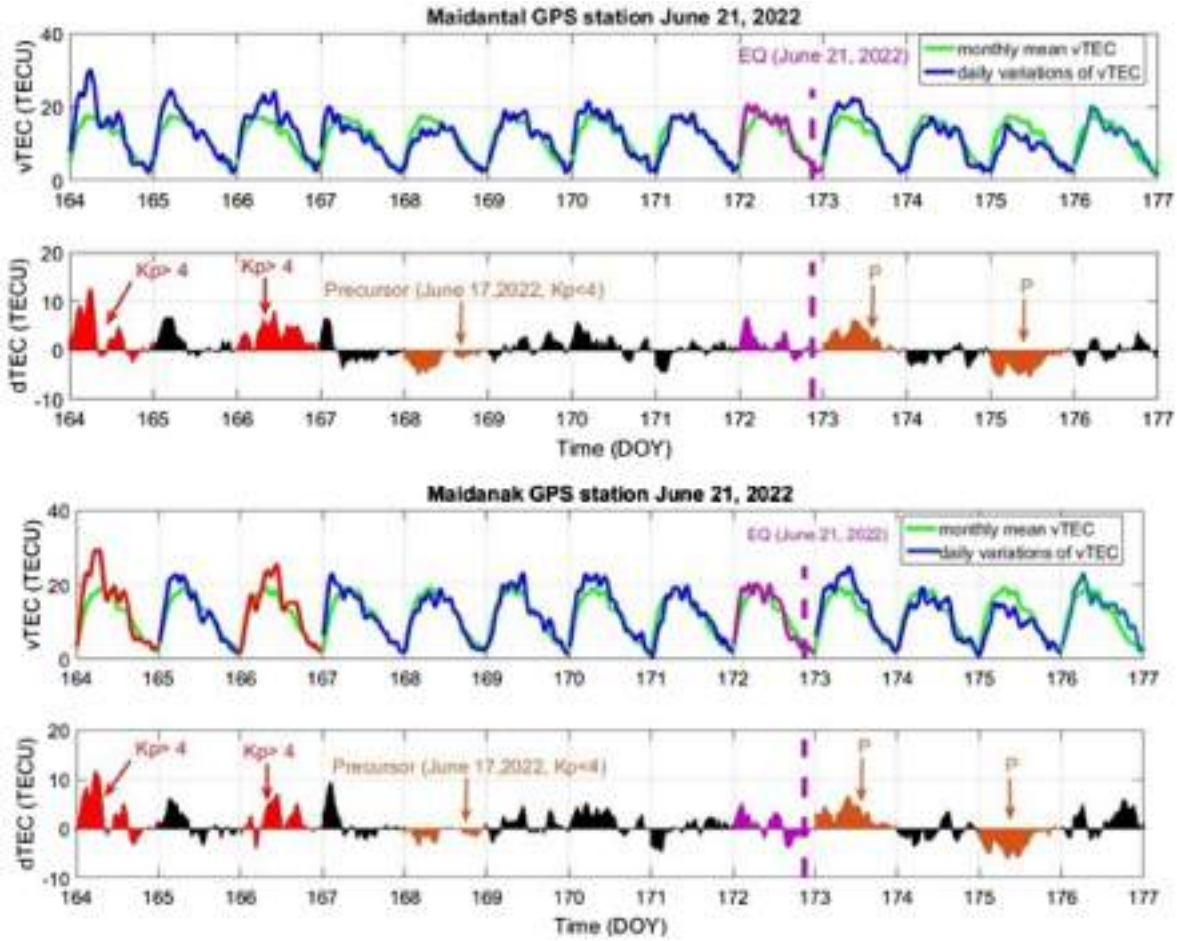

Figure 6
Vertical and Differential TEC variations above Maidantal on top and Maidanak on the bottom for Afghanistan EQ on June 21,2022 in comparison with the monthly mean. P character denotes the precursor day. The Red line denotes the Kp index

Accordingly, anomalies were not identified as ionospheric precursors of earthquakes if the Kp index exceeded 4.

4.1. Faraday Rotation

Analogous calculations for the group delay can be performed in order to find the Faraday rotation angle of the polarization plane of the propagating wave due to the inequality of the speeds of propagation of left-polarized and right-polarized wave components. The angle of Faraday rotation is determined by the difference of real parts of refractive indexes for left and right polarized waves. The sign of the rotation angle is dependent on the collision frequency of plasma particles. The main contribution to Faraday rotation gives the upper part of the ionosphere, where collision frequency is not large and the angle of rotation has a positive sign. The expression for Faraday rotation $\Delta\psi$ angle on the ray path interval Δs looks like

$$\Delta\psi = \frac{2\pi e^3}{cm^2}\frac{NB\cos\theta}{\omega^2 - \Omega_e^2\cos^2\theta}\Delta s, \qquad (20)$$

where $\Omega_e = (e/mc)B$ is the gyrofrequency of the electrons in plasma, and θ is the angle between the directions of the wave propagation and magnetic field. For the radio wave frequencies $\omega \gg \Omega_e$, one

can find an expression for the resulting angle of Faraday rotation as the integral

$$\psi = \frac{e^3}{2\pi cm}\frac{1}{f^2}\int_s NB\cos\theta ds = 2.365\times 10^4 f^{-2}\int n_e B\cos\theta ds. \quad (21)$$

The dependence of Faraday rotation angle on height is the same as of L_1. But in application to GPS monitoring, the effect is too small due to the great values of used frequencies. For example in assumption that the geomagnetic field is directed upward and for parameters $f = 1.57\times 10^9$ Hz, $B\sim 100$ G the maximum value of Faraday rotation angle is of the order of 10^{-5}. Faraday rotation of the polarization plane of the wave could be significant for experiments with smaller frequencies.

4.2. Doppler Frequency Shift

The next effect we examine is the Doppler frequency shift. When an object or any other source of waves moves in space, the frequency of the detected signal differs with the frequency of the emitted signal. This phenomenon, called as the Doppler frequency shift, is further amplified by inhomogeneities in space. The emitted and detected frequencies will differ on a value Ω_D, which can be also expanded in a series by degrees of the small parameter $v_m = \max|v|$ as

$$\Omega_D = \Omega_0 + \Omega_1 + \Omega_2 + \ldots. \quad (22)$$

Here Ω_0 is the Doppler frequency shift in vacuum which is equal to

$$\Omega_0 = \omega^0 v_\parallel / c, \quad (23)$$

where $v_\parallel$ is the radial velocity of the source and ω^0 is the emitted wave frequency. The general expression for Ω_1 looks like

$$\Omega_1 = \frac{\omega^0}{2c}\left[v(\mathbf{R},t)v_\parallel + \frac{v_\perp}{R}\int_0^R \nabla v(s,t)sds + \int_0^R \frac{\partial v(s,t)}{\partial t}ds\right], \quad (24)$$

where $v_\perp$ is the transversal with respect to undisturbed ray component of the source velocity. Ω_1 consists of three parts: (1) first is determined by the local value of v in the point of source (satellite) location; (2) second appeared because in close moments signal propagates through close but different points of inhomogeneous space; (3) the third part is connected with dependence of space parameters on time. Since the velocity of the inhomogeneities are rather small and much smaller than the speed of sound one can neglect the third part of the Ω_1. The first part and a non-vanishing component of the second part after averaging in space and with the help of the Eqs. (13) and (16) can be written as

$$\Omega_1 = \Omega_{1\parallel} + \Omega_{1\perp} = -\frac{\pi e^2}{cm\omega}0.05N_m\left[v_\parallel e^{-\frac{z_h}{H}} + v_\perp\left(\frac{z_h+H}{z_h}e^{-\frac{z_h}{H}} - \frac{H}{z_h}\right)\right]. \quad (25)$$

Assuming angle β to be small one can neglect $v_\parallel$ in comparison with $v_\perp$, which in this case is approximately equal to the satellite velocity. $\Omega_{1\perp}$ as a function of z_h is graphically presented in Fig. 7.

The graph has a maximum at the point $z_h = 200$ km, it corresponds to the height of approximately 600 km from the surface of the Earth. The value of $\omega\sim 10^7 Hz$. For GPS measurements, the effect is typically negligible due to the high frequencies used and the high altitude of the satellite's motion.

5. Possible VLF Radio Signal Anomaly Associated with the Tashkent Earthquake on 22 August 2008

5.1. The Stanford University VLF Receiver at Tashkent Station and Transmitters

The VLF receiver is located at the Ulugh Beg Astronomical Institute in Tashkent (Geographic Lat. (N) 41° 19′ 5427″, Long. (E) 69° 17′ 7671″). Operating since May 2008, the equipment used is the Stanford VLF radio receiver, also known as the Atmospheric Weather Electromagnetic System for Observation, Modeling, and Education (or AWESOME), designed to capture natural and man-made signals in the frequency range between 500 Hz and 47 kHz (Barr et al., 2000; Cohen et al., 2009; Scherrer et al., 2008; Zhu et al., 2022).

The data is recorded with two orthogonal air-core wire loop antennae, each sensitive to one component of the horizontal magnetic field, enabling for

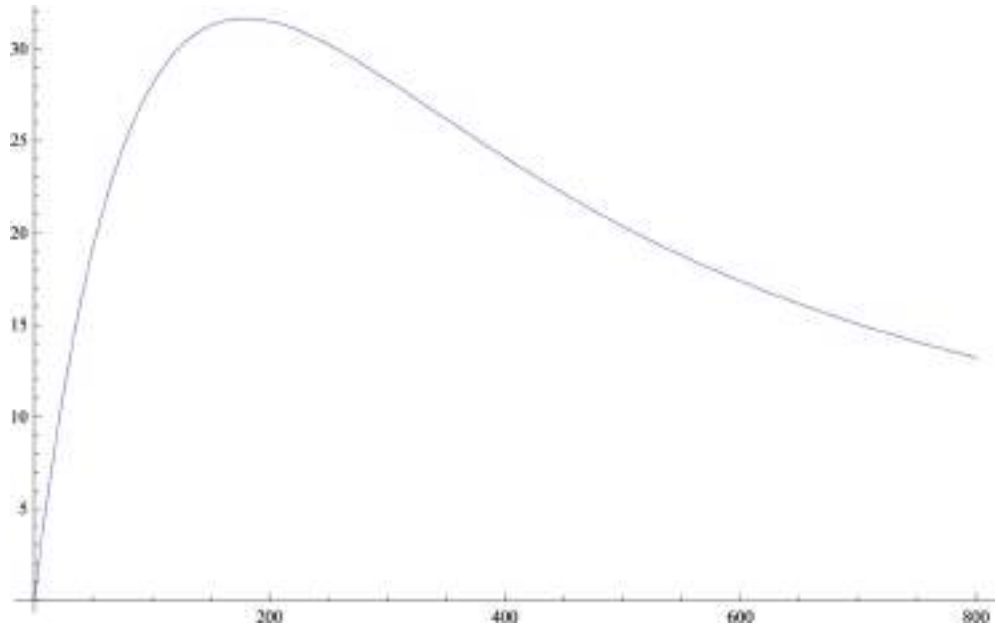

Figure 7
The dependence of the first correction to Doppler shift of the electromagnetic wave, propagating through the inhomogeneities of the highest layer of the ionosphere, from height

directional information extraction (Dai et al., 2023; Du & Wang, 2013; Yin et al., 2023; Zhou et al., 2022a, 2022b). VLF signals induce voltages in the wire loop antennae, albeit at extremely small magnitudes (ranging from 100 s of femtovolts to picovolts). Consequently, low-noise amplification is required in order to extract these signals effectively. To achieve this, a preamplifier, depicted adjacent to the loops in the accompanying figure photograph, is positioned outdoors alongside the antenna.

Following amplification, the signal travels along a cable to a line receiver box, which is typically indoors next to a computer. Within the line receiver, an anti-aliasing filter is aplied, and the signal is synchronized with GPS timing to ensure absolute timing accuracy of 100–200 ns. Using a phase-locked loop, the 1 PPS GPS signal is used to generate a 100 kHz sampling signal, which is fed into a PCI card inside the computer which digitizes and stores the data from both antennae. Software developed by Stanford sets the schedule for recording. On the basis of the best reception at the receiver and taking into account the most convenient radio paths, the following transmitters were selected in the year 2008: GQD (f = 22.1 kHz, United Kingdom), HWU (f = 20.9 kHz, France), DHO (f = 23.4 kHz, Germany), NRK (f = 37.5 kHz, Iceland), NAA (f = 24 kHz, USA), ICV (f = 20.27 kHz, Italy) and NSC (f = 45.9 kHz, Italy). The transmitters-receiver distance ranges from 500 to 3500 km. A number of nations currently operate large VLF transmitters. Most of the energy radiated by such VLF transmitters is trapped between the ground and the lower ionosphere, forming the Earth-ionosphere waveguide. Subionospheric VLF signals reflect from the D-region of the ionosphere, probably the least studied region of the Earth's atmosphere. These altitudes (70–90 km) are too far for balloons and too low for satellites, making in-situ measurements extremely rare. The only possible method of probing this D region is VLF sub-ionospheric radio signals (Fig. 8).

5.2. *VLF Data Analysis*

Any variations on the ionospheric D—region lead to changes in the propagation conditions for VLF waves propagating subionospherically, and hence changes in the observed amplitude and phase of

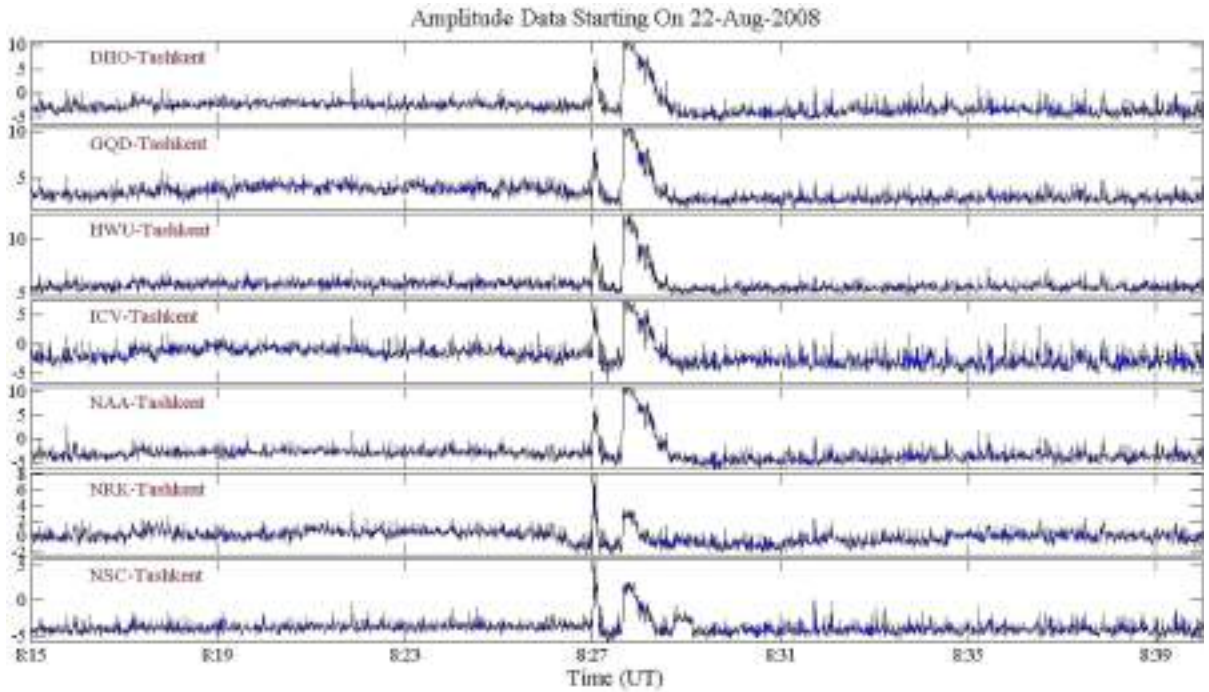

Figure 8
The amplitudes of radio signals from the different paths measured by VLF receiver in Tashkent from 08.15 to 08.40 UT on 22-Aug-2008

VLF transmissions are due to different kinds of perturbation sources; (1) solar flares, (2) geomagnetic storms (and the corresponding particle precipitation), (3) the direct effect of lightning. Subionospheric VLF measurements are particularly responsive to the study of this altitude range due to the fact that the nighttime reflection height is in the vicinity of 85 km altitude. Measurements of the amplitude and phase of VLF signals propagating in the earth-ionosphere waveguide have long been used effectively for remote sensing of the ionosphere (Sorokin et al., 2006a).

Two different primary types of sub-ionospheric Very Low Frequency (VLF) signatures have been identified resulting from the lightning activity, namely (i) the so-called Early/fast VLF conductivity changes in which the sub ionospheric VLF signal amplitude/phase changes (Inan et al., 1988 and references therein) within <20ms of the causative lightning flash, indicating an immediate effect of the lightning discharge in the overlying lower ionosphere, and (ii) VLF signatures of lightning-induced electron precipitation (LEP) events, in which the sub ionospheric VLF signal/amplitude changes after an onset delay of $\sim$ 1 s with respect to the causative lightning flash, consistent with the finite wave and particle travel times respectively to/from the regions of maximum cyclotron resonant pitch angle scattering of the energetic (>100keV) radiation belt particles which causes them to precipitate into the lower ionosphere (Inan et al., 1988). VLF remote sensing is a sensitive means for probing the lower ionosphere ($\sim$ 40 to 90 km altitude), used to measure celestial X-ray flares which might be monitored by observing annual phase variations on long VLF paths (Fishman & Inan, 1988).

We were the first to report a transient ionospheric disturbance from a gamma-ray burst, GB830801 which was one of the strongest bursts ever recorded up to that time. The observation path was from GBR (16 kHz) in England to Palmer Station in Antarctica. The more recent and more spectacular transient perturbation of VLF propagation created by a gamma-ray flare originating from a magnetar compact highly magnetized neutron star with the surface

magnetic field Gauss, known as a Soft Gamma Repeater (SGR)—(Inan et al., 1999, 2007). Transient amplitude changes of more than 20 dB and phase changes of $\sim 65^{\circ}$ were observed on the path from NPM in Hawaii to Palmer Station in Antarctica. A gigantic periodic flare from the soft gamma repeater SGR $1900 + 14$ produced enhanced ionization at ionospheric altitudes of 30 to 90 km, which was observed as unusually large amplitude and phase changes of very low frequency (VLF) signals propagating in the Earth-ionosphere waveguide. The VLF signals remained perturbed for $\sim$ 5 min and exhibited the 5.16 s periodicity of the giant flare detected on the Ulysses spacecraft. Quantitative analysis indicates the presence of an intense initial low energy (3–10 keV) photon component that was not detectable by the Ulysses instrument. In addition to these solar-terrestrial effects, we can suggest one more effect of earthquakes (or seismic activity) on the lower ionosphere.

6. Conclusions

In this study, we investigated the potential for earthquake prediction and identified several effects that could serve as earthquake precursors. In this paper, we analyzed GPS data from the Afghanistan earthquake and calculated the total electron content in the F-layer of the ionosphere. Ionospheric precursors were identified 4 days before the Afghanistan earthquake. We also derived an analytical solution for the scalar potential distribution in the lower ionosphere by selecting the expression of external upward electric current by the ejection of charged aerosols from the ground before earthquakes. This solution enabled us to uncover additional energy losses of radio waves propagating through this region of the ionosphere. Furthermore, we explored periodic inhomogeneities in electron concentration in the upper ionosphere by the influence of the propagating waves. By approximating these inhomogeneities with periodic functions, we obtained first-order corrections to the group delay, Faraday rotation angle, and Doppler frequency shift of propagating waves. We discussed the potential utility of these corrections in practical measurements. Notably, our findings suggest that the first correction to the group delay of the wave holds significant promise for practical application in earthquake prediction, particularly through GPS monitoring of the ionosphere. The theoretical analysis provided measurable values for the group delay variation of GPS signals propagating through the upper ionosphere in the context of earthquakes. Similarly, the correlation is found between electron density measurements obtained by satellites moving in the upper ionosphere and variations observed in GPS observations before the earthquakes. Although the effects of Faraday rotation and Doppler shift may be relatively small at GPS frequencies, they could still be useful in observations involving fewer frequencies.

Acknowledgements

We are grateful to Stanford STAR laboratory members in particular to Umran Inan, Morris Cohen, Ben Cotts, and Naoshin Haque for involving us in the ionospheric study, for fruitful discussions and explanations in the process of work, for comments, and for help in improving the of the paper.

Author contributions H.E., B.A, M.S.: Conceptualization, Methodology, Software, Data curation, Writing - Original draft preparation, Visualization,Validation. D.B., P.J. : Visualization, Investigation, Writing- Original draft preparation. A.M.M: Writing- Investigation, Reviewing and Editing. All authors read and approved the final manuscript.

Funding

Not applicable.

Data Availability

Not applicable.

Declarations

Competing interests The authors declare no competing interests.

Conflict of Interest The authors declares no conflict of interest.

Informed Consent Statement Not applicable.

Publisher's Note Springer Nature remains neutral with regard to jurisdictional claims in published maps and institutional affiliations.

References

Ahmedov, B. J., Tojiev, S. R., & Eshkuvatov, H. E. (2015). Low radiofrequency radiation in the D-layer of the ionosphere and the possibility of their registration on Tashkent VLF station. *Uzbek Journal of Physics, 17*(6), 339–350.

Barr, R., Llanwyn Jones, D., & Rodger, C. J. (2000). ELF and VLF radio waves. *Journal of Atmospheric and Solar-Terrestrial Physics, 62*, 1689–1718.

Biagi, P.F., Castellana, L., Maggipinto, T., Loiacono, D., Augelli, V., Schiavulli, L., Ermini, A., Capozzi, V., Solovieva, M.S., Rozhnoi, A.A., Molchanov, O.A. & Hayakawa, M. (2008) Disturbances in a VLF radio signal prior to the M=4.7 offshore Anzio (central Italy) earthquake on 22 August 2005 Natural Hazards and Earth System Sciences, **8**, 1041–1048. www.nat-hazards-earth-syst-sci.net/8/1041/2008/.

Biagi, P.F., Castellana, L., Maggipinto, T., Maggipinto, G., Minafra, A., Ermini, A., Capozzi, V., Perna, G., Solovieva, M., Rozhnoi, A., Molchanov, O. A., and Hayakawa, M. (2007). Decrease in the electric intensity of VLF/LF radio signals and possible connections. Natural Hazards and Earth System Sciences, 7, 423–430, http://www.nat-hazards-earth-syst-sci.net/7/423/2007/.

Burgess, W. C., & Inan, U. S. (1993). The role of ducted whistlers in the precipitation loss and equilibrium flux of radiation belt electrons. *Journal of Geophysical Research, 98*(A9), 15643–15665.

Calais, E., & Minster, J. B. (1998). GPS, earthquakes, the ionosphere, and the space shuttle. *Physics of the Earth and Planetary Interiors, 105*, 167–181.

Chmyrev, V. M., Isaev, N. V., Serebryakova, O. N., Sorokin, V. M., & Sobolev. (1997). Small-scale plasma inhomogeneities and correlated ELF emissions in the ionosphere over an earthquake region. *Journal of Atmospheric and Solar-Terrestrial Physics, 59*, 967–973.

Cohen, M. B., Inan, U. S., & Paschal, E. W. (2009). Sensitive broadband ELF/VLF radio reception with the AWESOME instrument. *IEEE Transactions on Geoscience and Remote Sensing*. https://doi.org/10.1109/TGRS.2009.2028334

Dai, Z., Li, X., & Lan, B. (2023). Three-dimensional modeling of tsunami waves triggered by submarine landslides based on the smoothed particle hydrodynamics method. *Journal of Marine Science and Engineering, 11*(10), 2015. https://doi.org/10.3390/jmse11102015

Du, W., & Wang, G. (2013). Intra-event spatial correlations for cumulative absolute velocity, arias intensity, and spectral accelerations based on regional site conditions. *Bulletin of the Seismological Society of America, 103*(2A), 1117–1129. https://doi.org/10.1785/0120120185

Eshkuvatov, H. E., Ahmedov, B. J., Tillayev, Y. A., Arslan Tariq, M., Libo Liu, M., & Shah, A. (2023). Ionospheric precursors of strong earthquakes observed using six GNSS stations data during continuous five years (2011–15). *Geodesy and Geodynamics, 14*(1), 65–79.

Fishman, G. J., & Inan, U. S. (1988). Observation of an ionospheric disturbance caused by a gamma-ray burst. *Nature, 331*, 418–420.

Hayakawa, M., Horie, T., Yoshida, M., Kasahara, Y., Muto, F., Ohta, K., Nakamura, T. (2008). On the ionospheric perturbation associated with the 2007 Niigata Chuetsu-oki earthquake, as seen from sub ionospheric VLF/LF network observations, Natural Hazards and Earth System Sciences, **8**, 573–576, www.nat-hazards-earth-syst-sci.net/8/573/2008/.

Hayakawa, M. (2007). VLF/LF radio sounding of ionospheric perturbations associated with earthquakes. *Sensors, 7*, 1141–1158.

Hayakawa, M., Ohta, K., Maekawa, S., Yamauchi, T., Ida, Y., Gotoh, T., Yamaguchi, N., Sasaki, H., & Nakamura, T. (2006). Electromagnetic precursors to the 2004 Mid-Niigata Prefecture earthquake. *Physics and Chemistry of the Earth, 31*, 356–364.

Horie, T., Maekawa, S., Yamauchi, T., & Hayakawa, M. (2007a). A possible effect of ionospheric perturbations associated with the Sumatra earthquake, as revealed from sub ionospheric very-low-frequency (VLF) propagation (NWC-Japan). *International Journal of Remote Sensing, 28*(13), 3133–3139.

Horie, T., Yamauchi, T., Yoshida, M., & Hayakawa, M. (2007b). The wave-like structures of ionospheric perturbation associated with Sumatra earthquake of 26 December 2004, as revealed from VLF observation in Japan of NWC signals. *Journal of Atmospheric and Solar-Terrestrial Physics, 69*, 1021–1028.

Inan, U. S., Lehtinen, N. G., Lev-Tov, S. J., Johnson, M. P., Bell, T. F., & Hurley, K. (1999). Ionization of the lower ionosphere by gamma-rays from a magnetar: Detection of a low energy (3–10 keV) component. *Geophysical Research Letters, 26*(22), 3357–3360.

Inan, U. S., Lehtinen, N. G., Moore, R. C., Hurley, K., Boggs, S., Smith, D. M., & Fishman, G. J. (2007). Massive disturbance of the daytime lower ionosphere by the giant γ-ray flare from magnetar SGR 180620. *Geophysical Research Letters, 34*, L08103. https://doi.org/10.1029/2006GL029145

Inan, U. S., Shafer, D. C., Yip, W. Y., & Orville, R. E. (1988). Subionospheric VLF signatures of nighttime D-region perturbations in the vicinity of lightning discharges. *Journal of Geophysical Research, 93*(A10), 11455–11427.

Kasahara, Y., Muto, F., Horie, T., Yoshida, M., Hayakawa, M., Ohta, K., Rozhnoi, A., Solovieva, M., Molchanov, O.A. (2008). On the statistical correlation between the ionospheric perturbations as detected by sub ionospheric VLF/LF propagation anomalies and earthquakes, Natural Hazards and Earth System Sciences 8, 653–656, www.nat-hazards-earth-syst-sci.net/8/653/2008/.

Liu, J. Y., Chuo, Y. J., Shan, S. J., Tsai, Y. B., Chen, Y. I., Pulinets, S. A., & Yu, S. B. (2004). Pre-earthquake ionospheric anomalies

registered by continuous GPS TEC measurements. *Annales Geophysicae, 22*, 1585–1593.

Mareev, E. A., Iudin, D. I., and Molchanov, O. A. (2002) Mosaic source of internal gravity waves associated with seismic activity, in: Seismo Electromagnetics: Lithosphere-Atmosphere-Ionosphere Coupling, edited by: Hayakawa, M. and Molchanov, O., TERRAPUB, Tokyo, 249–253.

Molchanov, O., Rozhnoi, A., Solovieva, M., Akentieva, O., Berthelier, J. J., Parrot, M., Lefeuvre, F., Biagi, P. F., Castellana, L., and Hayakawa, M. (2006) Global diagnostics of the ionospheric perturbations related to the seismic activity using the VLF radio signals collected on the DEMETER satellite, Natural Hazards and Earth System Sciences, 6, 745–753, http://www.nat-hazards-earth-syst-sci.net/6/745/2006/.

Molchanov, O.A., Hayakawa, M. (2008). Seismo-electromagnetics and related phenomena: History and latest results, TERRAPUB, Tokyo, 189p.

Molchanov, O. A., & Hayakawa, M. (2001). VLF monitoring of atmosphere–ionosphere boundary as a tool to study planetary waves evolution and seismic influence. *Physics and Chemistry of the Earth Part C, 26*, 453–458.

Pulinets, S., & Boyarchuk, K. (2004). *Ionospheric precursors of earthquakes*. Springer.

Rapoport, Yu. G., Gotynyan, O. E., Ivchenko, V. N., Hayakawa, M., Grimalsky, V. V., Koshevaya, S. V., & Juarez-R, D. (2006). Modeling electrostatic-photochemistry seismoionospheric coupling in the presence of external currents. *Physics and Chemistry of the Earth, 31*, 437–446.

Rozhnoi, A., Molchanov, O., Solovieva, M., Gladyshev, V., Akentieva, O., Berthelier, J. J., Parrot, M., Lefeuvre, F., Hayakawa, M., Castellana, L., and Biagi, P. F.: Possible seismo-ionosphere perturbations revealed by VLF signals collected on ground and on a satellite, Natural Hazards and Earth System Sciences, 7, 617–624, 2007, http://www.nat-hazards-earth-syst-sci.net/7/617/2007/.

Scherrer, D., Cohen, M. B., Hoekesma, T., Inan, U. S., Mitchell, R., & Scherrer, P. (2008). Distributing space weather monitoring instruments and educational materials worldwide for IHY 2007: The AWESOME and SID project. *Advances in Space Research*. https://doi.org/10.1016/j.asr.2007.12.013

Shah, M., Abbas, A., Ehsan, M., et al. (2021a). Ionospheric–thermospheric responses in south America to the august 2018 geomagnetic storm based on multiple observations. *IEEE journal of Selected Topics in Applied earth Observations and Remote Sensing, 15*, 261–269.

Shah, M., Ahmed, A., Ehsan, M., Khan, M., Tariq, M. A., Calabia, A., & Rahman, Z. (2020). Total electron content anomalies associated with earthquakes occurred during 1998–2019. *Acta Astronautica, 175*(2020), 268–276. https://doi.org/10.1016/j.actaastro.2020.06.005

Shah, M., Aibar, A. C., Tariq, M. A., et al. (2020b). Possible ionosphere and atmosphere precursory analysis related to Mw> 6.0 earthquakes in Japan. *Remote Sensing of Environment, 239*, 111620.

Shah, M., Draz, M. U., & Saleem, T. (2023a). A comprehensive study on the synchronized outgoing longwave radiation and relative humidity anomalies related to global Mw $\geq$ 6.5 earthquakes. *Natural Hazards*. https://doi.org/10.1007/s11069-023-06262-w

Shah, M., Ehsan, M., Abbas, A., et al. (2021b). Possible thermal anomalies associated with global terrestrial earthquakes during 2000–2019 based on MODIS-LST. *IEEE Geoscience and Remote Sensing Letters, 19*, 1–5.

Shah, M., Ehsan, M., Abbas, A., et al. (2022). Possible thermal anomalies associated with global terrestrial earthquakes during 2000–2019 based on MODIS-LST. *IEEE Geoscience and Remote Sensing Letters, 19*, 1–5. https://doi.org/10.1109/LGRS.2021.3084930

Shah, M., Inyurt, S., Ehsan, M., Ahmed, A., Shakir, M., Ullah, S., & Shahid Iqbal, M. (2020a). Seismo ionospheric anomalies in Turkey associated with M $\geq$ 6.0 earthquakes detected by GPS stations and GIM TEC. *Advances in Space Research, 65*(11), 2540–2550. https://doi.org/10.1016/j.asr.2020.03.005

Shah, M., & Jin, S. G. (2015). Statistical characteristics of seismo-ionospheric GPS TEC disturbances prior to global Mw$\geq$ 5.0 earthquakes (1998–2014). *Journal of Geodynamics, 92*, 42–49. https://doi.org/10.1016/j.jog.2015.10.002

Shah, M., Khan, M., Ullah, H., & Ali, S. (2018). thermal anomalies prior to the 2015 Gurkha (Nepal) earthquake from MODIS land surface temperature and outgoing longwave radiations. *Geodynamics & Tectonophysics., 9*(1), 123–138. https://doi.org/10.5800/gt-2018-9-1-0341

Shah, M., Qureshi, R. U., Khan, N. G., et al. (2021c). Artificial Neural Network based thermal anomalies associated with earthquakes in Pakistan from MODIS LST. *Journal of Atmospheric and Solar Terrestrial Physics, 215*, 105568.

Shah, M., Shahzad, R., Jamjareegulgarn, P., et al. (2023). Machine-learning-based lithosphere-atmosphere-ionosphere coupling associated with Mw > 6 earthquakes in America. *Atmosphere (basel), 14*, 1236. https://doi.org/10.3390/atmos14081236

Shah, M., Tariq, M. A., Ahmad, J., Naqvi, N. A., & Jin, S. (2019b). Seismo ionospheric anomalies before the 2007 M7.7 Chile earthquake from GPS TEC and DEMETER. *Journal of Geodynamics, 127*, 42–51.

Shah, M., Tariq, M. A., & Naqvi, N. A. (2019a). Atmospheric anomalies associated with Mw>6.0 earthquakes in Pakistan and Iran during 2010–2017. *Journal of Atmospheric and Solar-Terrestrial Physics*. https://doi.org/10.1016/j.jastp.2019.06.003

Shvets, A., Hayakawa, M., & Maekawa, S. (2004). Results of subionospheric radio LF monitoring prior to the Tokachi (M = 8, Hokkaido, 25 September 2003) earthquake. *Natural Hazards, 4*, 647–653.

Sorokin, V. M. (2007). Plasma and electromagnetic effects in the ionosphere related to the dynamics of charged aerosols in the lower atmosphere. *Russian Journal of Physical Chemistry B, 1*(2), 138–170.

Sorokin, V. M., Chmyrev, V. M., & Isaev, N. V. (1998). A generation model of small-scale geomagnetic field-aligned plasma inhomogeneities in the ionosphere. *Journal of Atmospheric and Solar-Terrestrial Physics, 60*, 1331–1342.

Sorokin, V. M., Chmyrev, V. M., & Yaschenko, A. K. (2001). Electrodynamic model of the lower atmosphere and the ionosphere coupling. *Journal of Atmospheric and Solar-Terrestrial Physics, 63*, 1681–1691.

Sorokin, V. M., Chmyrev, V. M., & Yaschenko, A. K. (2005a). The theoretical model of DC electric field formation in the ionosphere stimulated by seismic activity. *Journal of Atmospheric and Solar-Terrestrial Physics, 67*, 1259–1268.

Sorokin, V. M., Isaev, N. V., Yaschenko, A. K., Chmyrev, V. M., & Hayakawa, M. (2005b). Strong DC electric field formation in the low latitude ionosphere over typhoons. *Journal of Atmospheric and Solar-Terrestrial Physics, 67*, 1269–1279.

Sorokin, V. M., & Yaschenko, A. K. (2000). Electric field disturbance in the earth-ionosphere layer. *Advances in Space Research, 26*, 1219–1223.

Sorokin, V. M., Yaschenko, A. K., Chmyrev, V. M., & Hayakawa, M. (2006a). DC electric field amplification in the mid-latitude ionosphere over seismically active faults. *Physics and Chemistry of the Earth, 31*, 447–453.

Sorokin, V. M., Yaschenko, A. K., Chmyrev, V. M., & Hayakawa, M. (2006b). DC electric field formation in the mid-latitude ionosphere over typhoon and earthquake regions. *Physics and Chemistry of the Earth, 31*, 454–461.

Tojiev, S., Ahmedov, B., & Eshkuvatov, H. (2014). Ionospheric precursors of earthquakes recorded by VLF receiver at Tashkent IHY station. *Advances in Space Research, 54*, 628–643.

Tojiev, S. R., Ahmedov, B. J., Tillayev, Y. A., & Eshkuvatov, H. E. (2013). Ionospheric anomalies of local earthquakes detected by GPS TEC measurements using data from Tashkent and Kitab stations. *Advances in Space Research, 52*, 1146–1154.

Tojiev, S. R., Morozova, V. S., Ahmedov, B. J., & Eshkuvatov, H. E. (2012). *Electromagnetic studies of ionospheric and magnetospheric perturbations associated with the earth* (pp. 254–278). Atmospheric and Astrophysical Phenomena.

Yin, L., Wang, L., Li, J., Lu, S., Tian, J., Yin, Z., & Zheng, W. (2023). YOLOV4_CSPBi: Enhanced land target detection model. *Land, 12*(9), 1813. https://doi.org/10.3390/land12091813

Zhou, G., Zhao, D., Zhou, X., Xu, C., Liu, Z., Wu, G., & Zou, L. (2022a). An RF amplifier circuit for enhancement of echo signal detection in bathymetric LiDAR. *IEEE Sensors Journal, 22*(21), 20612–20625. https://doi.org/10.1109/JSEN.2022.3206763

Zhou, G., Zhou, X., Li, W., Zhao, D., Song, B., Xu, C., & Zou, L. (2022b). Development of a lightweight single-band bathymetric LiDAR. *Remote Sensing, 14*(22), 5880. https://doi.org/10.3390/rs14225880

Zhu, W., Chen, J., Sun, Q., Li, Z., Tan, W., & Wei, Y. (2022). Reconstructing of high-spatial-resolution three-dimensional electron density by ingesting SAR-derived VTEC Into IRI model. *IEEE Geoscience and Remote Sensing Letters, 19*, 2. https://doi.org/10.1109/LGRS.2022.3178242

(Received May 18, 2024, revised June 13, 2024, accepted June 28, 2024)

Results in Optics 16 (2024) 100717

Contents lists available at ScienceDirect

Results in Optics

journal homepage: www.sciencedirect.com/journal/results-in-optics

Use of educational technologies in teaching the basics of nanophysics, nanomaterials and nanotechnologies

Dilfuza Begmatova [a], Husan Eshkuvatov [a,b,*], Nuraddin Abdullayev [a], Nasiba Xodjayeva [a], Oqila Suvonova [a], Javlon Ishtayev [c]

[a] National University of Uzbekistan, University St. 4, Tashkent 100174, Uzbekistan
[b] "TIIAME" National Research University, Kori Niyoziy 39, Tashkent 100000, Uzbekistan
[c] Uzbek State University of Physical Education and Sport, Tashkent region, Chirchiq city, sportchilar street, house 19, Uzbekistan

ARTICLE INFO

Keywords:
Subject matter of nanophysics
Nanomaterials

ABSTRACT

In this article, we used modern technologies to teach the topic of nanomaterials and nanotechnologies. One of the main tasks of the development of modern nanotechnologies and nanomaterials is one of the main tasks of the development of nanoscale solid, liquid and gas phase structures and systems.

1. Introduction

Therefore, in acquiring knowledge about the basics, objects and subject matter of nanophysics and nanomaterials, it is important to analyze nanotechnologies in obtaining nano-sized materials, learn about the role of nanophysics (Berne et al., 2008; Bryan et al., 2007), and pay attention to the following in terms of dimensions (Daly and Bryan, 2007). Therefore, in acquiring knowledge about the basics, objects and subject matter of nanophysics, nanomaterials, it is important to analyze nanotechnologies in obtaining nano-sized materials, learn about the role of nanophysics (Berne et al., 2008; Bryan et al., 2007; Daly and Bryan, 2007; Dieter Vollath Nanoparticles-Nanocomposites-Nanomaterials, 2013; НаноМатериалы, 2007), and pay attention to the following in terms of dimensions (Нанотехнологии, 2008).

The word "nanotechnology" is a combination of the terms "nano" and "technology", and the suffix nano is from the Greek "nannos" – "tiny", which means one billionth (10–9) of a unit, for example, a meter (nanometer – nm). Considering that the size of atoms is 0.1–0.4 nm, a structure of 1 nm consists of dozens of atoms. For example, given that the diameter of a gold atom is 0.288 nm, the diameter of a cubic gold nanoparticle consisting of 13 gold atoms is 0.86 nm. There are three gold atoms (0.28 x 3 = 0.86) on each side of the cube, and 12 out of 13 atoms (92.3 %) are located on the surface of the nanoparticle. If we continue this operation and place the third layer, the size of the nanoparticle will reach 2 nm and the total number of atoms will be 147. The share of atoms on the surface is 62.6 percent. When the number of layers reaches 100, the nanoparticle diameter is 29 nm, the number of atoms is 3 million, and the percentage of atoms on the surface is only 3 percent.

At the moment, the integrity of nanosciences is expressed as follows:

Nanomaterials are unique materials formed based on nanosciences and nanotechnologies, which differ from traditional materials by their surface activity and functional properties.

This, in turn, indicates that there are differences in the types of nanomaterials and can be expressed as follows.

The fact that nanosciences and nanomaterials are products of nanotechnologies requires a deeper understanding of the nature of nanotechnologies. Nanotechnology is a set of methods for manufacturing products with a certain atomic structure, by arranging their atoms and molecules. According to this definition of nanotechnology, a natural question arises: can we manipulate (work here) materials at the level of atoms and molecules? The most beautiful way to solve this puzzle was proposed by Eric Drexler in his book "Building Machines". To work with atoms, he created special nanomachines or assemblers.

The direction of sciences based on nanotechnology is focused on the creation of nanomaterials (Fig. 1) (Нанотехнологии, 2008).

The production of nanomaterials is based on the bottom-up, that is, the formation of nanostructures from atomic and molecular structures, and on the contrary, the formation of nanostructures from top-down microscale structures (Fig. 2).

The Greek philosopher Democritus can be considered the grandfather of nanotechnology. He was the first to use the word "atom" 2400 years ago to describe the smallest particle of matter. Swiss physicist Albert Einstein proved in his work published in 1905 that the size of a

* Corresponding author.
E-mail address: husan@astrin.uz (H. Eshkuvatov).

https://doi.org/10.1016/j.rio.2024.100717
Received 18 March 2024; Received in revised form 30 May 2024; Accepted 16 June 2024
Available online 21 June 2024

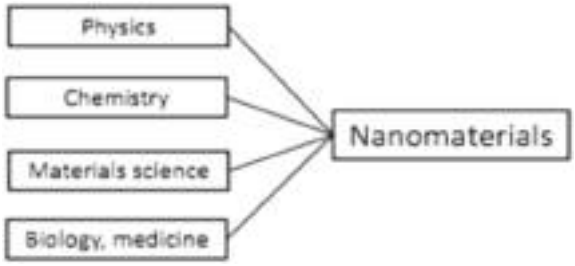

Fig. 1. Nanotechnology sciences and nanomaterials integration.

sugar molecule is approximately 1 nm.

In 1931, German physicists Max Knoll and Ernst Ruska created the electron microscope for the first time to study nano-objects. In 1959, the American physicist Richard Feynman announced his work that predicted the future of miniaturization. The fundamentals of nanotechnology were outlined in his famous lecture at the California Institute of Technology called There's Plenty of Room at the Bottom. Feynman scientifically confirmed that things can be made directly from atoms in terms of the basic laws of physics.

At that time, his words sounded like fiction for only one reason: the technology to perform operations on certain atoms (that is, to identify an atom, take it and put it in another place) did not yet exist. To increase interest in this field, Feynman promised $1,000 to the first person to write a page of the book on the tip of a needle. This was done in 1964. In 1968, Alfred Cho and John Arthur, employees of the scientific department of the American Bell company, developed the theoretical basis of nano-processing of the surface. In 1974, the Japanese physicist Norio Taniguchi introduced the word "nanotechnics" to the list of scientific terms and proposed to call the mechanisms (equipment) whose size is less than 1 μm. In 1981, German physicists Gerd Binnig and Heinrich Rohrer created the scanning tunneling microscope. They received the Nobel Prize 4 years later. In 1985, American physicists Robert Kerl, Harold Croteau, and Richard Smalley created a technology that can accurately measure objects with a diameter of 1 nm.

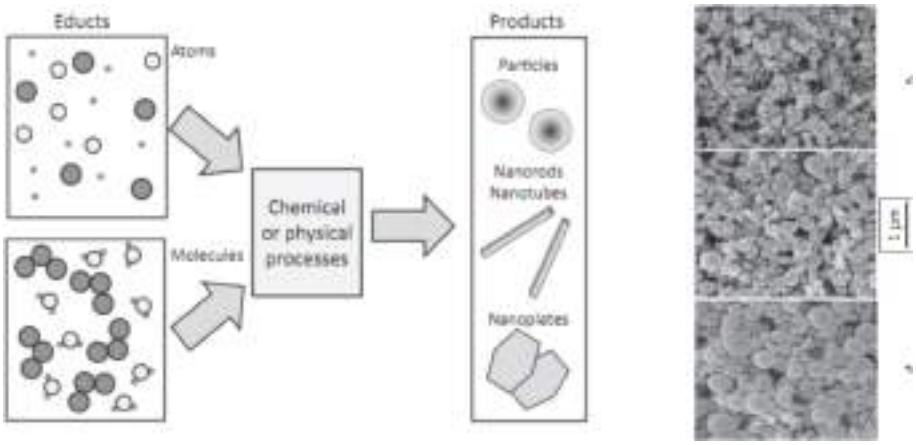

Fig. 2. Obtaining nanomaterials by physical and chemical methods.

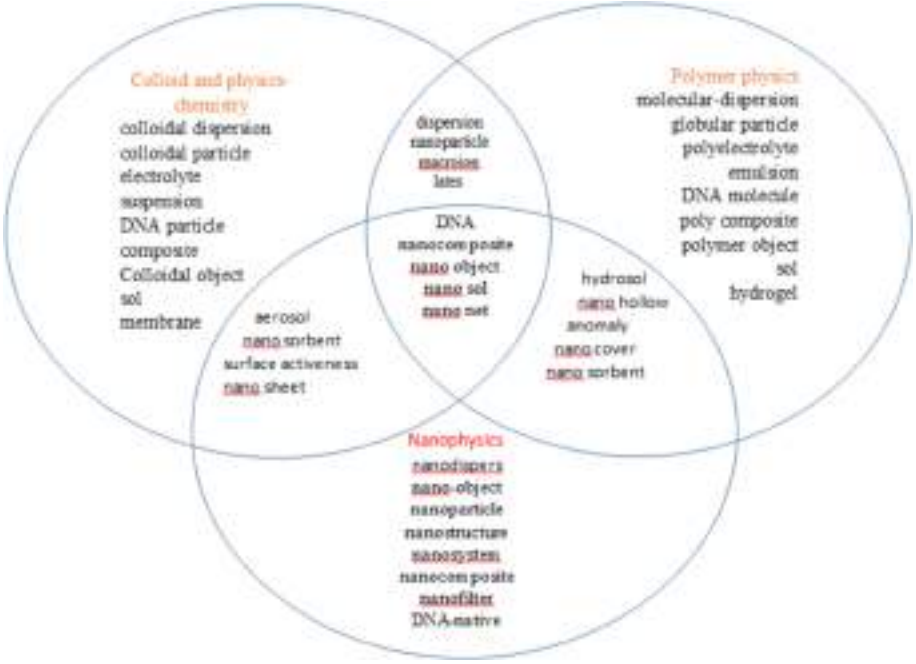

Fig. 3. A Venn diagram based on nanophysics and related sciences.

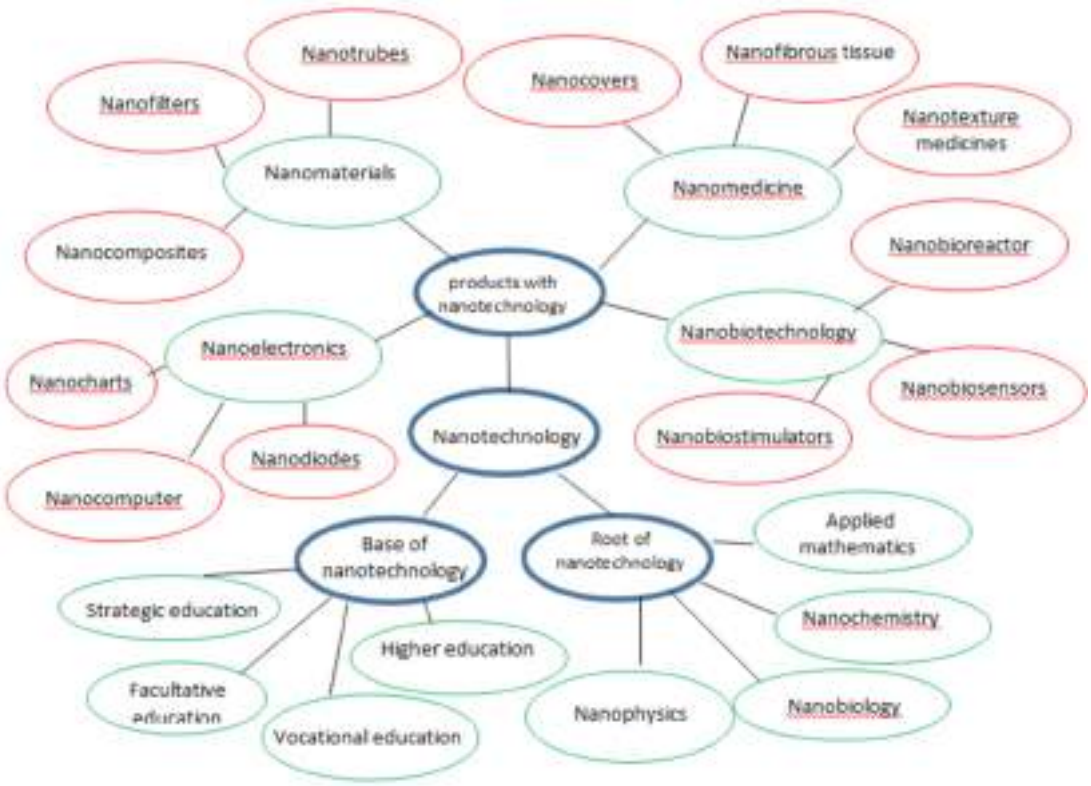

Fig. 4. A cluster representing the essence, roots and products of nanotechnology.

In 1986, unlike the tunneling microscope, an atomic force microscope was created that could interact with all materials. In 1986, nanotechnology became known to the general public. American futurologist Eric Drexler published a book predicting the rapid development of nanotechnology shortly. In 1989, IBM employee Donald Eigler wrote his company name with xenon atoms (Нанотехнологии. Азбука для всех. Под ред. акад. Ю.Д.Третьякова. М.: ФизМатлит, 2008).

In 1998, the Dutch physicist Seez Dekker created the nanotransistor. In 2000, the US government announced the National Nanotechnology Initiative. At that time, 500 million from the US federal budget. dollar was paid. In 2002, this amount was 604 million. increased to dollars. 710 million by 2003. dollars, in 2004 the US government allocated 3.7 billion dollars for 4 years to research in this field. allocated dollars. In general, the amount invested in the study of this field in the whole world is 12 billion amounts to a dollar! In 2004, the US government now considered the National Nanomedicine Initiative as part of the National Nanotechnology Initiative. This rapid development of nanotechnologies has resulted from the public's desire to absorb large amounts of information.

Modern silicon chips (integrated circuits) will continue to get smaller until around 2012 due to various technical requirements. But when the width of the passage is 40–50 nm, quantum mechanical distortions increase: electrons begin to pierce the passageways of transistors due to the tunnel effect. This means a short circuit. To overcome this, instead of silicon, carbon nanochips with dimensions of a few nanometers could be used. Currently, great research is being conducted in this direction.

2. Methodology and results

Pedagogical educational technologies such as the "Venn diagram", "Cluster", "Categorization" table, "Fish skeleton", and "B/BX/B" table were selected in this "Fundamentals of nanophysics, nanomaterials and nanotechnologies" teaching. The principles of their practical application are given below.

2.1. *Venn diagram method*

This method is highly effective in understanding the commonalities and differences of science and its elements and parts with related sciences (Khudoyberdieva et al., 2024). As an example, the difference of nanophysics with polymer physics and colloidal physical chemistry is analyzed and represented by the Venn diagram presented in Fig. 3. This diagram is based on three-ring intersections, and within the rings formed at their intersections, general concepts and terms related to colloid physico-chemistry, polymer physics, and nanophysics are introduced, respectively. In this, the fact that some concepts and terms belong to all branches of science, and some are expressed as belonging to only two, as well as to only one science, shows how the science of nanophysics differs from other sciences.

2.2. *"Cluster" method*

The cluster method is based on the principle of classifying materials in a branched manner, which is useful in revealing how the components of science and technology are related to each other and integrated. Using this method, A. A graphic organizer was used to show how nanoscience and nanomaterials are related to nanotechnology, presented in the textbook "Nanomaterilovedenie" (Minsk, 2015) published by Vityaz. This graphic organizer is presented in its original form, representing the essence, roots, bodies and products of nanotechnology (МукиМов, 2016).

To consolidate the knowledge learned from it, a systematized organizer graph was created using the "Cluster" method. This graphic organizer is shown to the students and they are asked to reconstruct, explain and interpret the graphic. The structured "Cluster" method is presented below, which represents the basis, roots and products of nanotechnology. With the help of this cluster, the principles of interdependence and differentiation of concepts and terms are mastered (see Fig. 4).

2.3. "Categorize" table method

This method analyzes the acquired knowledge about the "advantages", "uncertainties", and "dangers" of nanotechnology given during the lecture. For this, the graphic material from the above-mentioned "Nanomaterialovedenie" tutorial was used. This graphic is shown below in its original form and the material in it is translated into Uzbek. The essence of this graphic organizer is a comparative comparison of positive and negative situations related to nanotechnology (Daly and Bryan, 2007). The laws of interaction of electromagnetic wave radiation with atoms and molecules in the pyridine molecule are studied in the following articles (Otajonov et al., 2023; Xolmuminov et al., 2020). The translation of the data in the graph is presented in the table below, and students can independently categorize them according to their essence. The justifications we encountered can be sorted out in two categories. The first one consists of pointing at the looming shortage of nanoscientists and nanotechnologists. Indeed some authors (ХолМуМинов, 2015; Zaynobiddinov et al., 2013; Подвигалкин, 2012) reproduce discussions involving some of the National Science Foundation members that put forward figures assessing the number of nanoscientists that would be needed in 2015.

Principal new technologies, products, services
Self-healing and self-learning machines out of control
Effective diagnosis and treatment of diseases, achieving life extension
Convenient household services, high indicators in spiritual recreation and sports
Socio-economic development
A new trend in the arms race
A sharp decrease in energy and material consumption
Reducing the need for natural resources
The environment can improve or deteriorate
According to the principles of bioethics, what is allowed from technical advances
Is there a logical limit to the use of nanotechnology? What is the relationship between consumption and moral approval?
Development is likely to be more or less stable
Orientation and attitude towards values may be lost
A nanoterrorist outbreak may occur

2.4. "fish skeleton" method

In this method, the concept is expressed in the interdependence of the basis and essence of the materials. The following graphic organizer representing the classification of nanotechnologies was used.

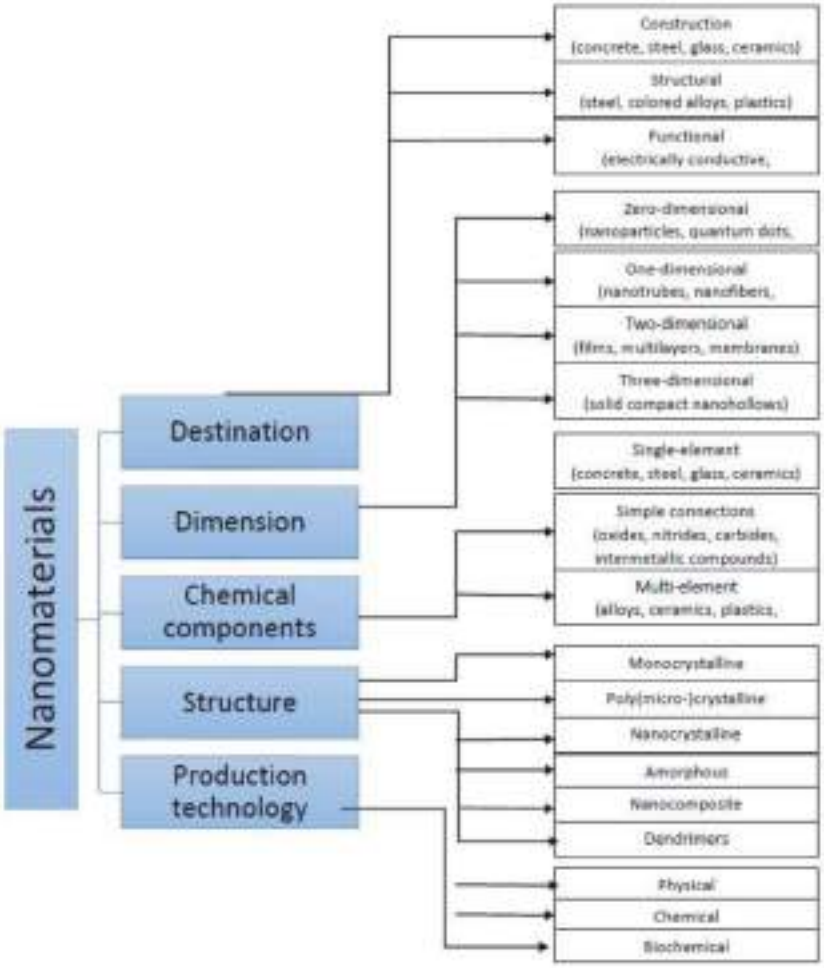

The information in the graph is translated and explained in depth using the educational technology method called “Fish Skeleton” below. In this, the cells on the lower parts of the fish skeleton are filled in and explained by the students.

In the drawing of the “fish skeleton” method, that is, “Nanotechnologies” is written on the head of the fish, and “nanomaterial” is concluded on the tail of the skeleton. Basic concepts of nanomaterials are written in the cells above the ribs of the skeleton. The meaning and essence of the above-mentioned concepts are written in the cells at the bottom of the skeleton. This process is repeated several times to a certain extent, and based on it, the interrelationships between nanotechnologies and nanomaterials are revealed, and what to pay attention to when obtaining nanomaterials by nanotechnologies is determined.

To strengthen the acquired knowledge and professional skills related to the basics of nanophysics, objects and subjects of nanophysics and nanomaterials and nanotechnologies in this lecture lesson, to remember and repeat the words, concepts, definitions and terms encountered during the lesson, as well as to bring them into a certain order, the following “B/BX” /B“ table method was used. It has categories such as ”B“ – I know, ”BX“ – I want to know, ”B“ – I know, which are presented sequentially in a table for convenient comparison. With its help, questions were prepared based on the materials of the lectures and included in the ”B/BX/B“ folder with the following partial changes.

2.5. “B/BX/B” table method

A partial modification of this method, that is, the table shows the column “Concepts, definition and lesson materials” by lesson. The student is required to express his opinion and attitude to the questions and opinions presented in this column.

Concepts, definitions and lesson materials	I know	I want to know	I have learned
Fundamentals of nanophysics			
Objects of nanophysics			
The subject of nanophysics			
Nanomaterials research methods			
Structures of nanomaterials			
Nanomaterials have unique and special properties			
Classifications of nanotechnologies			
Nanocomposites			
Nanocoatings			
Nanofibers			
Nanofilms			
Nanosorbents			

3. Conclusion

This article presents the foundational concepts of nanophysics, nanomaterials, and nanotechnologies through the application of educational technologies. These technologies are carefully selected to align with the specific nature and objectives of the lecture. By employing these methods, learners can actively and effectively assimilate knowledge and information on the subject matter.

CRediT authorship contribution statement

Dilfuza Begmatova: Writing – review & editing, Writing – original draft, Visualization, Validation, Supervision, Investigation. **Husan Eshkuvatov:** Software, Investigation, Formal analysis, Data curation, Conceptualization. **Nuraddin Abdullayev:** Resources, Project administration, Methodology, Investigation, Formal analysis, Data curation. **Nasiba Xodjayeva:** Data curation, Validation, Visualization. **Oqila Suvonova:** Data curation, Investigation, Methodology, Resources, Software. **Javlon Ishtayev:** Conceptualization, Data curation, Project administration, Validation.

Declaration of competing interest

The authors declare that they have no known competing financial interests or personal relationships that could have appeared to influence the work reported in this paper.

Data availability

The data that has been used is confidential.

References

Berne, R.W., 2008. Content and pedagogy for ethics education in nanoscale science and technology development. In: Sweeney, A.E., Seal, S. (Eds.), Nanoscale Science and Engineering Education. American Scientific Publishers, Valencia CA, pp. 547–566.

Bryan, L.A., Daly, S., Hutchinson, K., Sederberg, D., Benaissa, F., & Giordano, N. (2007). A design-based approach to the professional development of teachers in nanoscale science. Paper presented at the annual meeting of the National Association for Research in Science Teaching, New Orleans.

Daly, S., Bryan, L., 2007. Models of nanoscale phenomena as tools for engineering design and science inquiry. Proceedings of the American Society for Engineering Education.

Dieter Vollath Nanoparticles-Nanocomposites-Nanomaterials. An introduction for beginners. – Wiley-VCH Verlag GHbH &Co.KGaA, Boschstr. Weinheim, Germany, 2013. – P. 322.

Гусев А.И. НаноМатериалы, наноструктуры, нанотехнологии. М. ФизМатлит. 2007 г. 416 с.

Фостер Л. Нанотехнологии. Наука, инновации и возМоЖности. Техносфера, - Москва, : Наука. 2008 г. 120 с.

Нанотехнологии. Азбука для всех. Под ред. акад. Ю.Д.Третьякова. М.: ФизМатлит, 2008.

Khudoyberdieva, D., Otajonov, S., Eshchanov, B., Eshquvatov, H., Abdullayev, N., 2024. Mechanisms of Raman scattering spectrum of light from pyridine molecule in the lower frequency range. Results Opt. 16, 100685.

МукиМов К. Митти бунёдкор ёҳуд нанотехнологиялар ниМа? – Тошкент. :Университет. 2016. – 130 б.

Otajonov, S., Allaquliyeva, S., Eshchanov, B., 2023. Nuraddin abdullayev, husan eshkuvatov, manifestation of the laws of vibrational motion of molecules of the condensed medium under the influence of laser radiation in the raman spectrum. Results Opt. 13.

Xolmuminov A.A., Matyakubov B.M., Salimov Sh.M.Polimerlar fizikasi. Darslik. T.: O’zbekiston Respublikasi Milliy gvardiyasi Harbiy-texnik instituti, 2020. 233 bet.

ХолМуМинов А.А. ПолиМерлар физикаси. қув қўлланМа, Тошкент “Университет” 2015 й с. 195.

Zaynobiddinov, S.Z., Teshaboyev, A.T., Ismoilov, Q., 2013. Nanozarralar fizikasi, kimyosi va texnologiyalari. Toshkent.:fan. 338 c.

Подвигалкин Я., Музалев., П.А., Ушаков Н.М., НаноМатериалы и нанотехнология. Матлы электрон. Техн. 2012. № 2. С.51.